J Mater Sci (2012) 47:7860–7869
DOI 10.1007/s10853-012-6538-4

ULTRAFINE GRAINED MATERIALS

Microstructure and dislocation density evolutions in MgAlZn alloy processed by severe plastic deformation

Miloš Janeček · Jakub Čížek · Jenő Gubicza · Jitka Vrátná

Received: 9 March 2012 / Accepted: 26 April 2012 / Published online: 9 May 2012

Abstract Commercial MgAlZn alloy AZ31 was processed by hot extrusion and equal channel angular pressing (ECAP) known as EX-ECAP. Microstructure and defect structure evolution with strain due to ECAP were investigated by TEM, positron annihilation spectroscopy (PAS), and X-ray diffraction. Significant grain refinement was obtained by EX-ECAP. In the extruded condition relatively low density of dislocations was determined by PAS. Sharp increase of dislocation density occurred during the first two passes of ECAP, followed by the saturation and even a decline manifesting the dynamic recovery at higher strains. XRD line profile analysis confirmed the results of PAS with slightly higher values of dislocation densities in individual conditions. Detailed analysis of contrast factors allows to determine the type of dislocations and to draw conclusions about slip activation and its variations with strain. The influence of microstructure evolution on mechanical properties is discussed.

M. Janeček (✉) · J. Vrátná
Department of Physics of Materials, Faculty of Mathematics and Physics, Charles University, Prague, Czech Republic
e-mail: janecek@met.mff.cuni.cz

J. Čížek
Department of Low Temperature Physics, Faculty of Mathematics and Physics, Charles University, Prague, Czech Republic

J. Gubicza
Department of Materials Physics, Eötvös Loránd University, Budapest, Hungary

Introduction

Magnesium alloys are, namely due to their high specific strength, gaining a renewed interest for structural applications in automotive and aerospace industry where weight is a critical factor. However, the applications of Mg alloys are still limited, because of problems associated with limited ductility, relatively low strength, low creep and corrosion resistance, and low forming capability. The limited ductility is a consequence of the small number of independent easy glide primary slip systems and the much higher values of the critical resolved shear stress in other slip systems. The occurrence of strong deformation textures and stress anisotropy are another factors negatively influencing the possible applications of Mg alloys as structural components [1].

It is well-known that the properties of magnesium alloys may be improved by refining the grain size to submicrometer or even nanometer level [2–7]. A variety of new techniques have been proposed for the production an ultrafine grained (UFG) structure in materials, as e.g., high pressure torsion, accumulative roll-bonding, etc. Among these techniques, which introduce the severe plastic deformation (SPD) in the material, the equal channel angular pressing (ECAP) [8] has become the most popular and widely used method of grain refinement due its versatility and scalability.

ECAP is reported to activate the prismatic and pyramidal slip systems and the resulting texture changes re-activate the basal slip [9]. Multiple processing of the samples by ECAP leads to changes in properties and microstructure that are typically non-monotonous, exhibiting an extreme value after 3–5 passes through the die [10]. In order to understand the underlying processes a detail knowledge of microstructure, defect structure, and texture development is necessary.

The objective of this article is to investigate the microstructure and dislocation structure evolution in specimens processed by ECAP up to 12 passes and to correlate it with mechanical properties.

Experimental procedures

Commercial AZ31 alloy, with a nominal composition of Mg–3 %Al–1 %Zn in the initial as chill-cast condition as received from Dead sea magnesium was used in this investigation. The material was first extruded at $T = 350$ °C with an extrusion ratio of ER = 22 using a 630 t direct extrusion press. Billets of the dimensions $10 \times 10 \times 120$ mm were machined from the extruded bar. ECAP pressing was performed at 180 °C to reduce grain growth during pressing [11] following route Bc at the speed of 50 mm/min. A series of specimens up to the maximum equivalent strain of 12 (1, 2, 4, 8, and 12 passes) were processed.

Specimens for light and transmission electron microscopy (TEM) observation of the ECAP-generated microstructure were taken from the middle part of the billet perpendicular to the pressing direction. TEM foils were first mechanically polished and finally ion-polished using a Gatan PIPS^{TM} ion mill at 4 kV and an incidence angle of 4°. TEM investigations were performed with a Jeol 2000FX electron microscope operated at 200 kV.

A $^{22}Na_2CO_3$ positron source ($\sim$1.5 MBq) deposited on a 2 μm thick mylar foil was used in positron lifetime measurements. The source was always sandwiched between two identical samples of the studied alloy. The source contribution consists of two components with lifetimes of 368 ps (intensity 8 %) and 1.5 ns (intensity 1 %) which come from positrons annihilated in the source spot and in the covering Mylar foil, respectively. Positron lifetime measurements were carried out using a fast–fast spectrometer [12] with a time resolution of 150 ps (FWHM ^{22}Na). At least 10^7 positron annihilation events were accumulated in each positron lifetime spectrum which was subsequently decomposed into individual exponential components by a maximum likelihood procedure [13].

The X-ray line profiles were measured by a high-resolution rotating anode diffractometer (Nonius, FR 591) using Cu $K\alpha_1$ ($\lambda = 0.15406$ nm) radiation. Two-dimensional imaging plates detected the Debye–Scherrer diffraction rings. The line profiles were obtained as a function of the diffraction angle by integrating the two-dimensional intensity distribution along the rings at discrete angle values. The line profiles were evaluated by the convolutional multiple whole profile (CMWP) fitting analysis [14]. In this procedure, the diffraction pattern is fitted by the sum of a background spline and the convolution of the instrumental pattern and the theoretical line profiles related to the crystallite size, dislocations, and twin faults. Seventeen peaks of Mg were used in the fitting procedure. The theoretical profile functions used in this fitting procedure were calculated on the basis of a model of the microstructure, where the crystallites have spherical shape and log-normal size distribution.

Results and discussion

Microstructure evolution

Light microscopy

The microstructure changes in specimens subjected to ECAP were observed by light microscopy and TEM. The microstructure of AZ31 alloy in the initial condition is shown in Fig. 1. The microstructure consists of almost equiaxed grains with the average size of approximately 150–200 μm. Several twins are also seen in the micrograph.

Hot extrusion resulted in strong grain refinement. However, the microstructure of the specimen after the extrusion is rather inhomogeneous containing zones with coarse grains surrounded by fine grains. The typical example of the extruded specimen is shown in Fig. 2a. The bimodal character of the microstructure remained after the first two passes of the ECAP (see Fig. 2b and c). During further straining the fragmentation of coarse grains occurred resulting in almost homogeneous microstructure as shown in Fig. 2d which represents the typical microstructure in the specimen after 4 passes of ECAP. The homogeneous microstructure did not change significantly in specimens after 8 and 12 passes. However, the limited

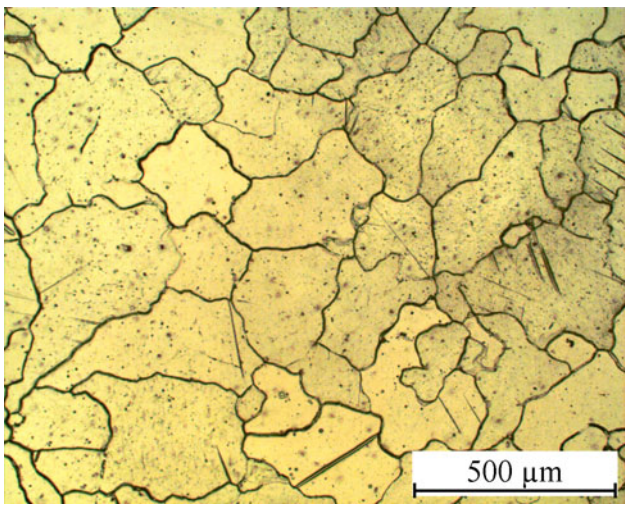

Fig. 1 Microstructure of the AZ31 alloy in the as-cast condition

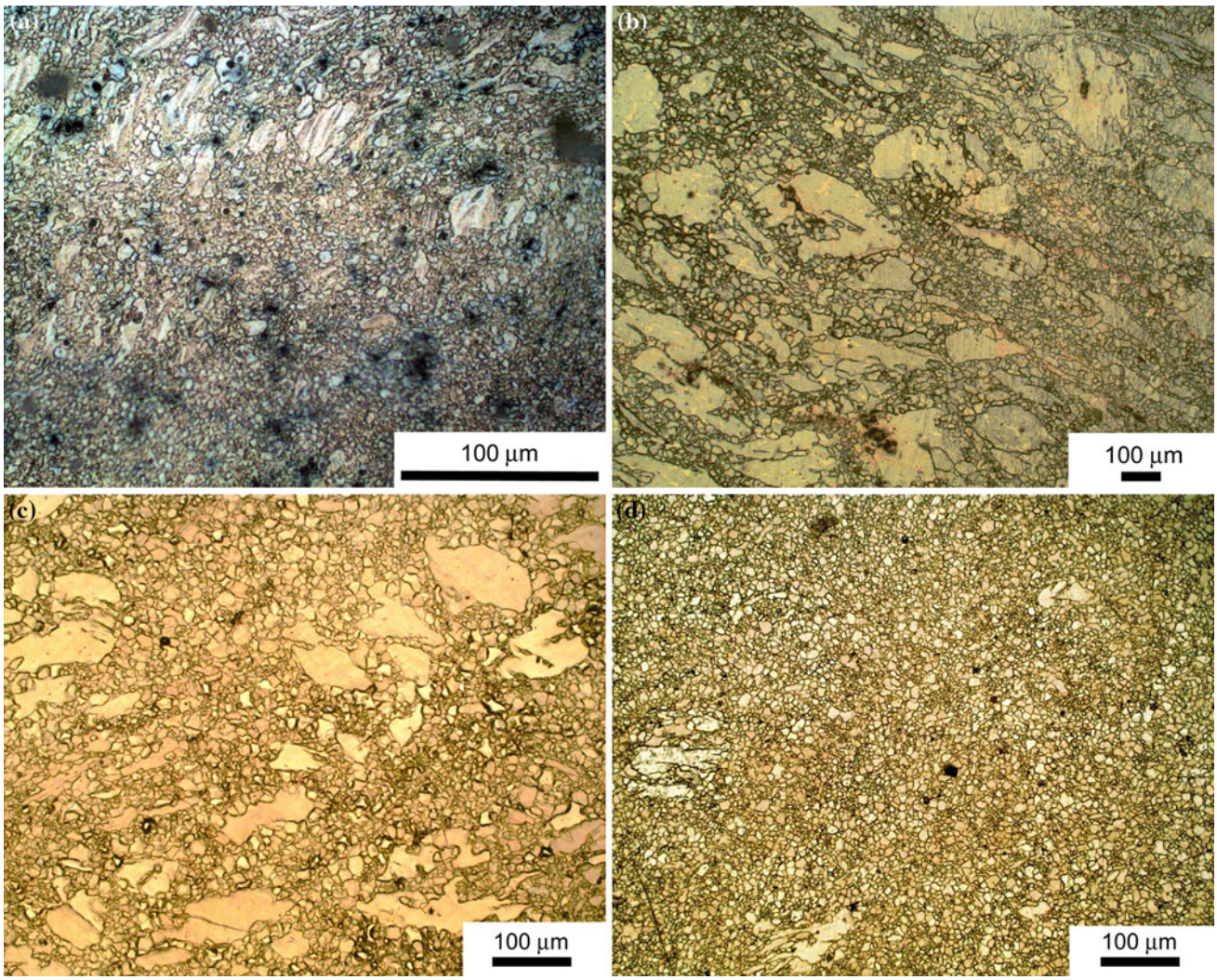

Fig. 2 Grain structure of the AZ31 alloy processed by ECAP from the extruded condition **a** extruded material, **b** after 1 pass, **c** after 2 passes, and **d** after 4 passes

resolution of the light microscope does not allow to characterize the details of microstructure changes.

Transmission electron microscopy

Detailed investigation of microstructure evolution and grain fragmentation with strain due to ECAP was performed by TEM. The typical microstructure of the extruded specimen is shown in Fig. 3a. It may be characterized as the heavily deformed structure with many dislocations which are inhomogeneously distributed within grains. Dislocations tend to rearrange themselves and form cell or subgrain boundaries. The initial stages of substructure formation were detected by a detail inspection of electron diffraction pattern variations throughout coarse grains. TEM observation confirmed the bimodal character of the microstructure observed by light microscopy. In Fig. 3b a zone surrounding a coarse grain is shown**.** The small grains having the size of several micrometers are clearly visible in the micrograph.

The microstructure in individual specimens after ECAP is shown in Fig. 4. The grain refinement occurred already during the first ECAP pass, see Fig. 4a where a zone containing fine grains is displayed. The average grain size of almost equiaxed grains is apparently below 1 µm with several grains having the size even below 500 nm. Only a small area fraction of large grains was left within the bimodal distribution. No significant grain size reduction was observed with increasing strain in zones with fine grains, cf. Fig. 4b, c, and d showing the microstructure in specimens after 2, 8, and 12 ECAP passes, respectively. On the other hand, in zones with coarse grains the increasing deformation caused the grain fragmentation and refinement. In the specimen after 8 passes almost homogeneous microstructure with equiaxed grains of the average size of approximately 500–600 nm was observed (see Fig. 4c).

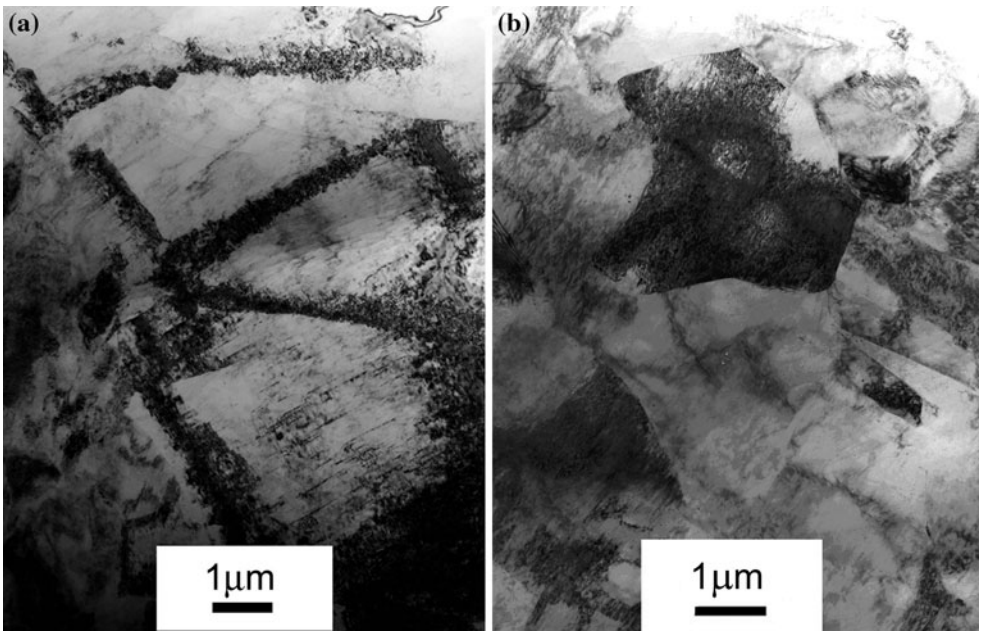

Fig. 3 TEM micrograph of AZ31 in extruded condition **a** Coarse grains. **b** Fine grains

The microstructure evolution and grain fragmentation in extruded specimen which underwent subsequent ECAP pressing corresponds well with observations of other authors in AZ31 alloy [5, 11, 12, 15] and confirms the principal differences of grain refinement in materials with hexagonal close packed (HCP) and face-centered cubic (FCC) lattice. In FCC metals, typically in Al, first the substructure is formed consisting of elongated bands of cells or subgrains. With increasing strain bands continuously evolve into an equiaxed UFG structure with the final grain size mostly given by the subgrain walls spacing [16]. Calculations of the shearing patterns for different processing routes lead to the conclusion that an equiaxed microstructure is achieved most rapidly in ECAP when slip occurs on three orthogonal planes over a wide range of angles following route Bc [17, 18]. On the other hand, grain refinement in magnesium alloys seems to be more complex and the formation of a bimodal grain structure after processing by ECAP was reported by many authors [19–21]. Bimodal distribution of grains is probably due to limited active slip systems in magnesium, therefore only favorably oriented grains are deformed and refined as first during ECAP process and areas of less deformed and larger grains are left in microstructure.

Defect structure evolution

The plastic shear deformation by the ECAP causes accumulation of large plastic strain and increase of structural defects. In this study we employed two techniques to characterize in detail the evolution of defects in individual specimens after ECAP.

Positron annihilation spectroscopy

Positron lifetime spectra of all samples studied can be well fitted by two exponential components. The shorter component with the lifetime τ_1, which is lower than the bulk positron lifetime in Mg $\tau_B = 225$ ps [22], represents a contribution of free positrons not trapped at defects. The longer component with lifetime $\tau_2 \approx 260$ ps arises from positrons trapped at dislocations [23].

The development of positron lifetimes τ_1, τ_2 with increasing number of ECAP passes is plotted in Fig. 5a, while Fig. 5b shows the dependence of the intensity I_2 of positron trapped at dislocations on the number of ECAP passes. The dislocation component with appreciable intensity of 20 % was detected already in the extruded alloy, i.e., prior to the ECAP processing. This testifies that dislocations were introduced into the alloy by plastic deformation during extrusion. The lifetime τ_2 of positrons trapped at dislocations remains approximately constant during ECAP processing confirming that the nature of positron traps does not change. The intensity I_2 of positrons trapped at dislocations first increases with increasing number of ECAP passes and becomes maximal in the specimen subjected to 2 passes. Further ECAP processing (more than 2 passes) causes a gradual decrease of I_2. Note that similar behavior of the intensity of dislocation component during ECAP processing was observed in other Mg alloys (AZ80, ZK60) [24].

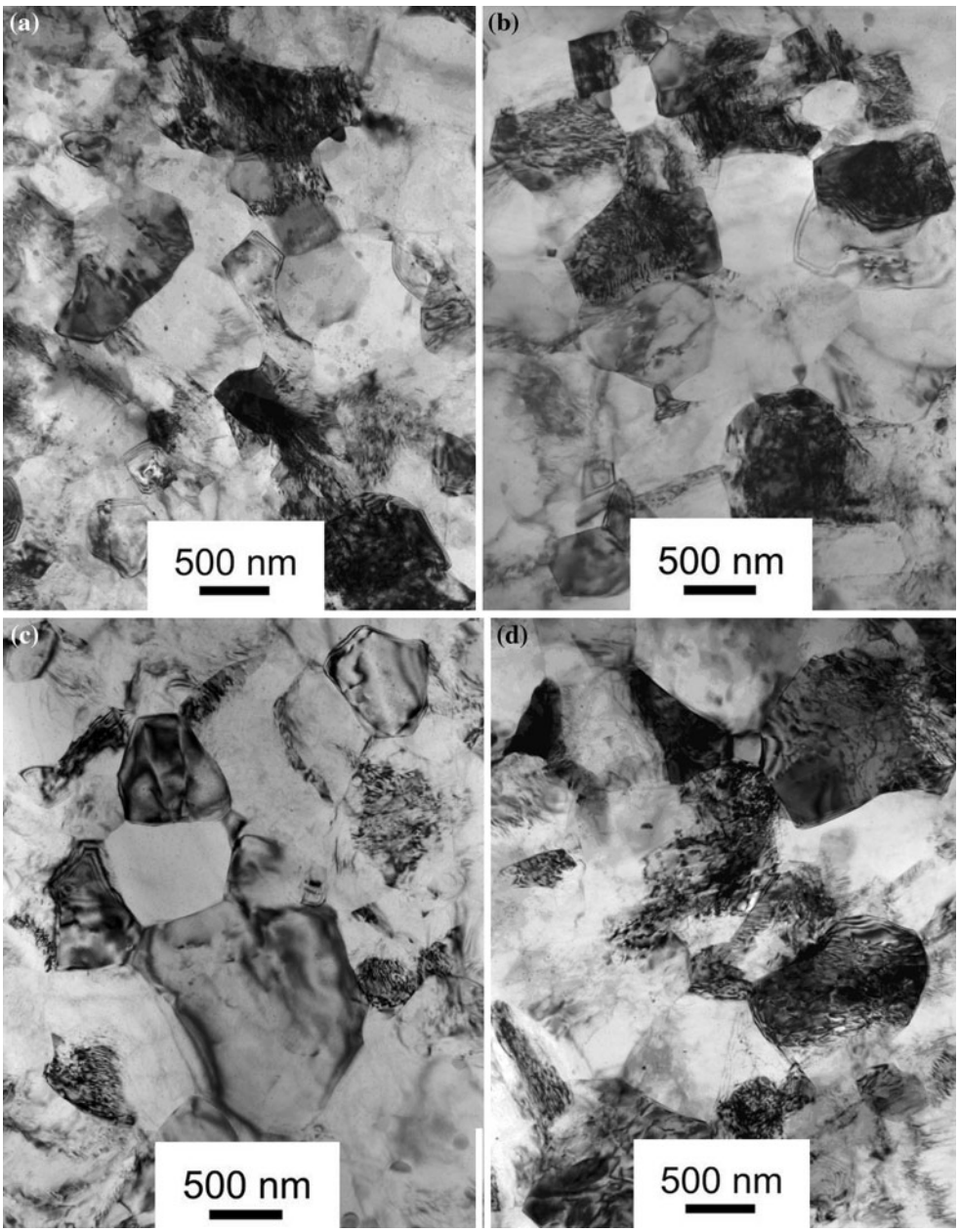

Fig. 4 TEM micrograph of specimens after ECAP **a** 1 pass, **b** 2 passes **c** 8 passes, and **d** 12 passes

The mean dislocation density ρ_D can be calculated from positron lifetime data using the two-state simple trapping model (STM) [25].

$$\rho_D = \frac{1}{v_D} I_2 \left(\frac{1}{\tau_1} - \frac{1}{\tau_2} \right). \quad (1)$$

The symbol v_D stands for the specific positron trapping rate to dislocations which in the majority of metals falls into the range of 10^{-5}–10^{-4} m^2 s^{-1} [26]. Here we used $v_D = 1 \times 10^{-5}$ m^2 s^{-1} since Mg exhibits low electron density in interatomic regions which makes the positron binding energy to open volume defects lower than in dense metals and, thereby, v_D is expected to be close to the lower limit of the aforementioned interval. Note that in the frame of the two-state trapping model the quantity

$$\tau_f = \left(\frac{I_1}{\tau_1} + \frac{I_2}{\tau_2} \right)^{-1} \quad (2)$$

equals to the bulk positron lifetime in the defect-free material. This relation was found to hold in all the specimens studied. This testifies that the alloys deformed by ECAP contain indeed a single type of defects and that dislocations are distributed relatively homogeneously in the specimens.

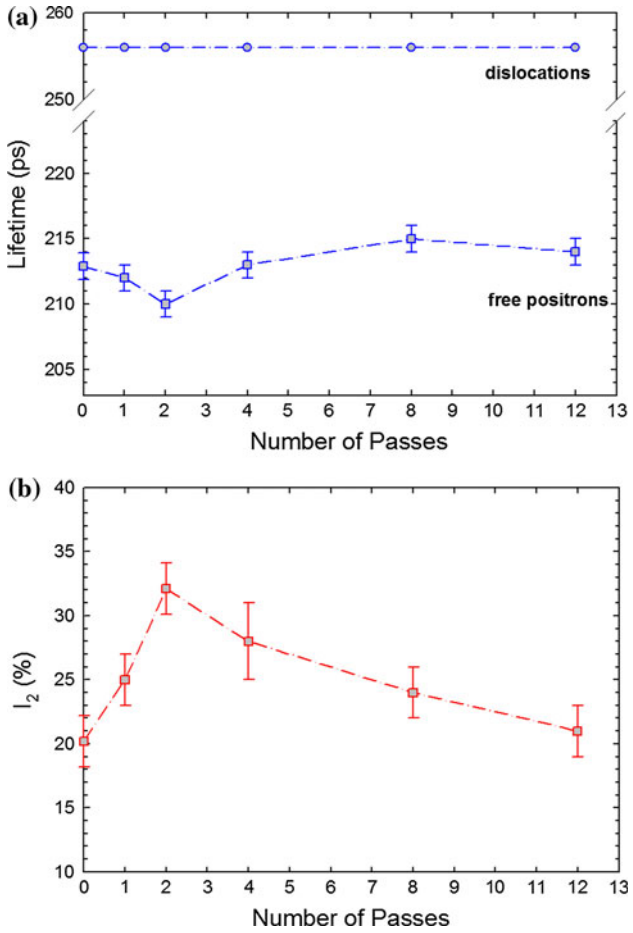

Fig. 5 Results of positron lifetime measurements for AZ31 alloy subjected to various number of ECAP passes. **a** Lifetimes τ_1 (squares) and τ_2 (circles) of the free positron and the dislocation component. **b** Intensity I_2 of the components arising from positrons trapped at dislocations

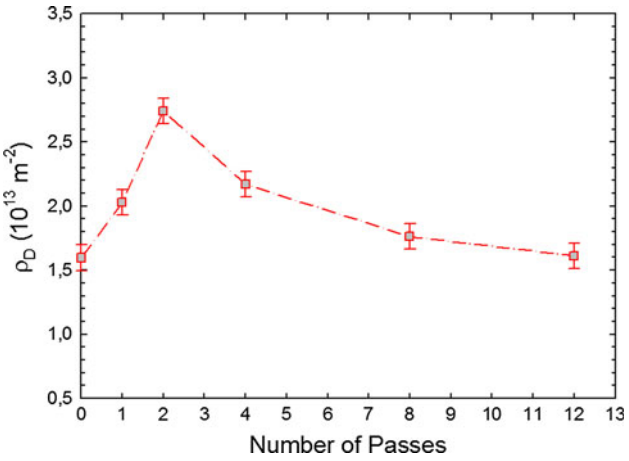

Fig. 6 Dislocation density ρ_D in AZ31 alloy subjected to various number of ECAP passes

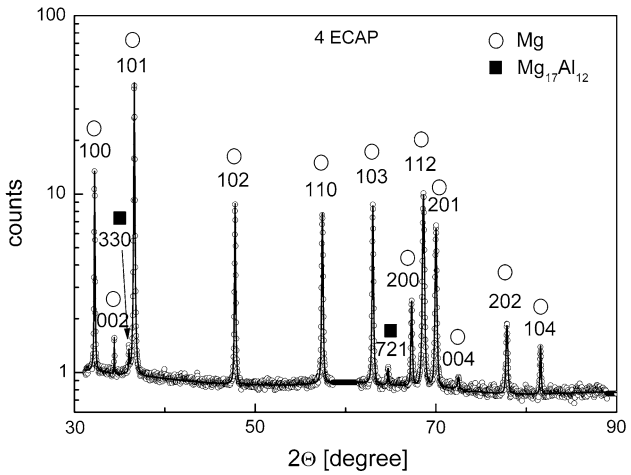

Fig. 7 CMWP fitting of the X-ray diffraction pattern in logarithmic intensity scale for AZ31 alloy processed by 4 passes of ECAP. The open circles and the solid line represent the measured and the fitted data, respectively. The indices of reflections for the Mg matrix and the $Mg_{17}Al_{12}$ phase are also indicated

The mean dislocation density ρ_D calculated from Eq. (1) is plotted in Fig. 6 as a function of the number of ECAP passes. One can see in Fig. 6 that ρ_D first increases during ECAP processing and reaches its maximum in the sample subjected to 2 ECAP passes. However, further ECAP processing leads to a gradual decrease of dislocation density indicating a recovery of dislocation structure connected with development of UFG structure. Most probably rearrangement of dislocations and mutual annihilation of dislocations with opposite sign takes place during further ECAP processing. Finally in the sample subjected to 12 ECAP passes ρ_D decreased to the similar value as in the extruded sample prior to ECAP processing.

X-ray diffraction

In Fig. 7, as an example, the CMWP fitting for AZ31 alloy processed by 4 passes of ECAP is shown. Open circles and the solid line represent the measured data and the fitted curves, respectively. The area-weighted mean crystallite size ($\langle x \rangle_{area}$), the density (ρ) and the character of dislocations as well as the twin boundary frequency (β) were determined by the line profile analysis. The area-weighted mean crystallite size was calculated from the median and the variance, m and σ, of the log-normal size distribution as $\langle x \rangle_{area} = m \exp(2.5\ \sigma^2)$ [27]. The twin boundary frequency is defined as the relative fraction of twin boundaries among the lattice planes acting as habit planes in twinning. In HCP materials twinning usually occurs on {101}, {102}, {111}, and {112} planes, therefore in the line profile analysis all of these twin families were considered. The relative fractions of different dislocation slip systems were determined by comparing the theoretical dislocation contrast factors with the experimental values using the procedure described in [28].

Table 1 The total integrated intensity of the X-ray diffraction peaks of $Mg_{17}Al_{12}$ phase relative to the intensity for the Mg matrix (I_{rel}), the area-weigthed mean crystallite size ($\langle x \rangle_{area}$), the dislocation density (ρ) and the relative fraction of screw dislocations in the Mg matrix

Sample	I_{rel} (%)	$\langle x \rangle_{area}$ (nm)	ρ (10^{14} m^{-2})	Fraction of screw dislocations (%)
Extruded	0	470 ± 80	0.9 ± 0.1	13 ± 13
1 ECAP	0.14 ± 0.03	173 ± 16	1.4 ± 0.1	60 ± 10
2 ECAP	0.14 ± 0.03	146 ± 15	1.7 ± 0.2	71 ± 5
4 ECAP	0.7 ± 0.1	134 ± 15	1.3 ± 0.1	47 ± 10
8 ECAP	2.6 ± 0.3	120 ± 13	1.1 ± 0.1	42 ± 17

The X-ray diffractograms revealed the existence of $Mg_{17}Al_{12}$ phase in addition to the Mg matrix. The amount of $Mg_{17}Al_{12}$ in the samples is characterized by its relative intensity in the diffractograms, i.e., the ratio of the integrated intensities of all $Mg_{17}Al_{12}$ and Mg peaks in the two theta range from 30 to 115 degrees. The values of the relative intensity (I_{rel}) are shown in Table 1. It is revealed that the amount of $Mg_{17}Al_{12}$ phase significantly increased with increasing number of ECAP passes. Most probably, before ECAP the majority of alloying elements were in solid solution and the ECAP processing at 180 °C caused the formation of $Mg_{17}Al_{12}$ precipitates.

Considerable twinning was not observed in any of the specimens. The practically zero value of the twin boundary frequency does not mean definitely the lack of twinning as the lowest detection limit of twin boundary frequency is about 0.05 % in the present experiments that corresponds to an average twin boundary spacing of about 400 nm. If the mean twin boundary spacing is higher than this value, line profile analysis gives practically zero value for twin boundary frequency. The low level of twinning is most probably caused by the relatively small size of crystallites formed during ECAP as in HCP metals the reduction of grain size is usually accompanied by the decrease of twinning activity [29]. The values of the crystallite size and the dislocation density are listed in Table 1. The crystallite size decreased up to 2 passes of ECAP then it remained unchanged within the experimental error. The dislocation density increased up to 2 passes then it decreased slightly when the number of ECAP passes increased. After 2 passes the reduction of the dislocation density along with the large increment of the amount of $Mg_{17}Al_{12}$ precipitates suggests that the alloying elements (Al and Zn) have stronger pinning effect on dislocations when they are solved in the matrix than in the form of precipitates. It is noted that the crystallite size determined by X-ray line profile analysis is smaller by a factor of about 4 than the grain size obtained by TEM. This phenomenon is well-known in the literature of SPD-processed metallic materials and can be attributed to the fact that the crystallites are equivalent to the coherently scattering domains. As the coherency of X-rays breaks even if they are scattered from volumes having quite small misorientations (1–2°), the crystallite size corresponds rather to the subgrain size in the severely deformed microstructures.

The dislocations in the different slip systems were evaluated for their edge/screw character. In this procedure, first the slip systems populated by dislocations were determined from the experimental dislocation contrast factors (q_1 and q_2) using the procedure described in [28]. In this method, the two experimental contrast factors were made equal to the weighted averages of the theoretical contrast factors for the eleven possible slip systems where the weights were one or zero for the populated or non-populated slip systems, respectively. Since the measured q values had experimental errors, their comparison with the theoretical contrast factors was carried out by introducing tolerances [28]. The evaluation procedure gave one or more sets of the eleven weights consisting of zero and one values as possible solutions. Finally, the values obtained for the screw dislocation slip systems in all solutions were summed up and divided by the sum of the values determined for all the slip systems. This number was used for the characterisation of the relative fraction of screw dislocations. Table 1 shows that the relative fraction of screw dislocations increased up to 2 passes then it decreased between 2 and 4 passes and remained unchanged between 4 and 8 passes. The Burgers-vector analysis of dislocations revealed that the majority of screw dislocations that disappeared for higher number of ECAP passes had Burgers-vectors of ⟨c⟩ and ⟨c+a⟩ types. The strong decrease of the fraction of ⟨c⟩ and ⟨c+a⟩ screw dislocations for higher number of ECAP passes can be explained by their high self-energy due to the large Burgers-vector and the easy occurrence of their cross-slip.

Comparison of dislocation density evaluated by PAS and XRD

Both experimental techniques revealed relatively high number of dislocations in all specimens. The dislocation density was found to increase up to 2 ECAP passes

followed by a continuous decline for higher strains; cf. Fig. 6 (PAS) and the Table 1 (XRD). Systematically higher absolute values of ρ_D (5–6 times) were obtained by XRD in all specimens. The reason is probably threefold:

First, both techniques employed theoretical models for the calculation of ρ_D. In case of PAS, it was the STM [25] which relies on the value of positron trapping rate ν_D (see Eq. 1). This value cannot be obtained experimentally and must be calculated from first principles and in metals falls within a certain range of values. The selection of the exact value was commented in the Section "Positron annihilation spectroscopy" The line profile analysis is also based on a microstructural model incorporated in the CMWP evaluation procedure [27].

Second, the signal obtained by both techniques yields information about the microstructure of different zones of the specimen. X-ray signal comes mostly from areas below the surface of the specimen while PAS signal from the bulk.

Third, both techniques employ numerical processing of experimental data and the results inevitably contain some error.

The reason of the difference in ρ_D obtained by both techniques is rather complex and its clarification requires further systematic studies. Let us treat the problem in relative units as there are the relative changes of ρ_D which should be independent of the technique, provided the evaluation is right. Let us take the specimen with the highest value of ρ_D as the reference, in our case the specimen after 2 ECAP passes, and determine relative changes of ρ_D with respect to the density $\rho_{D,max}$ in this specimen. The result is shown in Fig. 8 where the relative change $\rho_D/\rho_{D,max}$ is displayed as a function of the number of passes (strain). Excellent match of both curves corresponding to relative changes of dislocation density determined by PAS and XRD is clearly seen.

The course of this "master curve" describes unambiguously the evolution of dislocation density with strain during ECAP pressing. Significant increase of dislocation density with strain occurs during the first two ECAP passes. Almost double value of ρ_D was found in the specimen after 2 passes than in the extruded material. With increasing number of passes the dislocation density decreased and in the specimen after 12 passes it reached the value comparable with the extruded specimen.

In our previous study, we have found the similar non-monotonous dependence of dislocation density with strain also in other magnesium alloys [24] and explained it by dynamic recovery processes operating at higher strains. However, in other magnesium alloys, e.g., in AZ91, the monotonous increase of dislocation density with strain was found [30]. In this case, a high volume fraction of discontinuous $Mg_{17}Al_{12}$ precipitates having a rod-like shape were present in the alloy. During ECAP pressing these particles were continuously broken into smaller parts and their relatively homogeneous dispersion in the matrix contributed to further strengthening of the alloy due to increasing density of dislocations. These precipitates were also found in AZ31 alloy by XRD. However, their volume fraction was significantly lower and softening processes by rearrangement and recovery of dislocations at higher strains prevailed in this alloy.

Correlation of mechanical properties with microstructure evolution

Recently we investigated the mechanical properties of ultrafine grained AZ31 polycrystals processed by extrusion and ECAP [31]. In Fig. 9 the dependence of the yield stress on the number of passes is displayed. There is an obvious correlation between mechanical properties and the dislocation density evolution, cf. Figs. 8 and 9. Both $\sigma_{0.2}$ and ρ_D

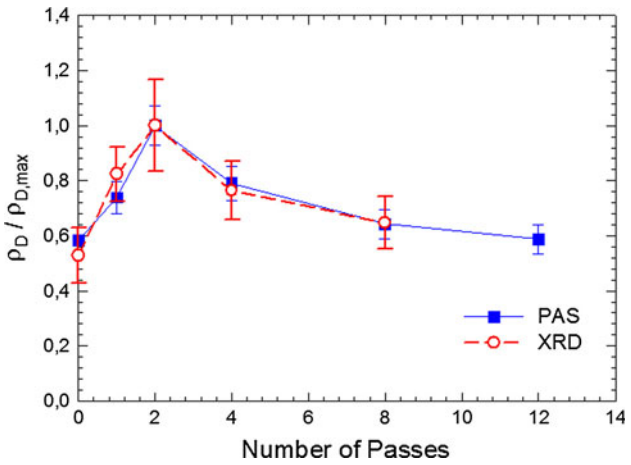

Fig. 8 The evolution of relative dislocation density in ECAPed specimens determined by PAS and XRD

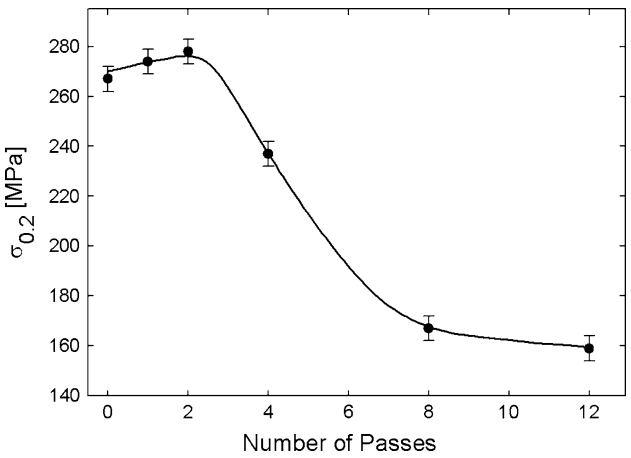

Fig. 9 The dependence of the yield stress on the number of ECAP passes

first increase with increasing strain up to 2 passes of ECAP where they reach the maximum and then decrease continuously with increasing strain.

The texture changes caused by ECAP process were also reported to have a crucial influence on the mechanical properties. As it was shown in our previous work [29], the initial extruded bars exhibit a strong basal texture, i.e., most grains have their crystallographic c-axis perpendicular to the extrusion direction. This orientation relation makes the {10.2} twinning mode difficult to activate, which belongs the one of the most important deformation mechanism in magnesium alloys [32]. The first and second pressing reorients the grains to twinning-proper direction. Since the {10.2} twinning causes hardening [32] and contributes to the strain accommodation [33], an increase in both strength and ductility is observed. The texture emerging after the fourth pass is again unsuitable for twinning [34], thus the plastic deformation is realized mostly by dislocation slip and a negative Hall–Petch relation is observed. The softening for higher passes is caused by prevailing impact of texture weakening over the strengthening effect of grain refinement [35]. Furthermore the dislocation density decreases with increasing pressing number as well, therefore the number of dislocation-type obstacles also decreases.

Our results indicate therefore that the influence of microstructure evolution during ECAP on mechanical properties is rather complex and may be explained both by dislocation structure or texture development. Strengthening due to grain refinement plays an important role only in early stages of pressing ($\varepsilon \leq 2$).

Conclusions

Microstructure and dislocation structure evolution with strain due to ECAP in extruded AZ31 alloy were investigated by light microscopy and TEM, positron annihilation spectroscopy and X-ray diffraction. The following conclusions may be drawn from this investigation:

- ECAP processing resulted in a strong grain refinement and a bimodal microstructure up to a strain of about 2,
- further ECAP pressing up to the strain of 4 caused the fragmentation of coarse grains while the fine grains were refined only slightly,
- Homogeneous distribution of almost equiaxed grains of the average size of 500 nm with equilibrium high-angle boundaries was observed only for high strains $\varepsilon \approx 8$.
- Dislocation density was found to increase with increasing strain up to $\varepsilon \approx 2$; for higher strain it declined continuously up to the value close to that of extruded specimen.
- The influence of microstructure on mechanical properties is rather complex controlled by dislocation density, texture and grain size evolution with strain due to ECAP.

Acknowledgements This study was financially supported by GACR under the grants 106/09/0482 and P108/10/0648. Partial support by Charles University Research Center "Physics of Condensed Matter and Functional Materials" is also acknowledged. One of the authors J.G. acknowledges financial support by the Hungarian Scientific Research Fund, OTKA, Grant No. K-81360 and by the European Union and the European Social Fund under grant agreement no. TÁMOP 4.2.1./B-09/1/KMR-2010-0003 and J.V. acknowledges financial support by GAUK 59409/2009 and SVV-265303.

References

1. Agnew SR, Horton JA, Lillo TM, Brown DW (2004) Scripta Mater 50:377
2. Kim HK, Lee YI, Chung CS (2005) Scripta Mater 52:473
3. Ishikawa K, Watanabe H, Mukai T (2005) J Mater Sci 40:1577. doi:10.1007/s10853-005-0656-1
4. Figueiredo RB, Langdon TG (2009) Int J Mater Res 100:843
5. Estrin Y, Yi SB, Brokmeier HG, Zuberova Z, Yoon SC, Kim HS, Hellmig RJ (1998) Int J Mater Res 99:50
6. Kulyasova O, Islamgaliev RK, Mingler B, Zehetbauer M (2009) Mater Sci Eng A503:176
7. Mingler B, Kulyasova OB, Islamgaliev RK, Korb G, Karnthaler HP, Zehetbauer MJ (2007) J Mater Sci 42:1477. doi:10.1007/s10853-006-0977-8
8. Segal VM (1995) Mater Sci Eng A 197:157
9. Gottstein G, Al Samman T (2005) Mater Sci Forum 495–497:623
10. Vrátná J, Stráský J, Janeček M, Král R (2009) In: Kainer KU (ed) Magnesium. Wiley-VCH, Weinheim, p 331
11. Figueiredo RB, Langdon TG (2009) Mater Sci Eng A501:105
12. Bečvář F, Čížek J, Lešták L, Novotný I, Procházka I, Šebesta F (2000) Nucl Instrum Methods Phys Res A 443:557
13. Procházka I, Novotný I, Bečvář F (1997) Mater Sci Forum 255–257:772
14. Ribárik G, Gubicza J, Ungár T (2004) Mater Sci Eng A 387–389:343
15. Bryla K, Dutkiewicz J, Malczewski P (2009) Arch Mater Sci Eng 40:17
16. Langdon TG (2007) Mater Sci Eng A462:3
17. Furukawa M, Iwahashi Y, Horita Z, Nemoto M, Langdon TG (1998) Mater Sci Eng A257:328
18. Furukawa M, Horita Z, Langdon TG (2002) Mater Sci Eng A332:97
19. Lapovok R, Cottam R, Thomson PF, Estrin Y (2005) J Mater Res 20:1375
20. Xia K, Wang JT, Wu X, Chen G, Gurvan M (2005) Mater Sci Eng A 410–411:324
21. Su CW, Lu L, Lai MO (2006) Mater Sci Eng A434:227
22. Čížek J, Procházka I, Smola B, Stulíková I, Kužel R, Matěj Z, Cherkaska V (2006) Phys Status Solidi (a) 203:466
23. Čížek J, Procházka I, Smola B, Stulíková I, Očenášek V (2007) J Alloys Compd 430:92
24. Müller J, Janeček M, Yi S, Čížek J, Wagner L (2009) Int J Mater Res 100:838
25. West R (1979) In: Hautojärvi P (ed) Positrons in solids. Springer-Verlag, Berlin, p 89

26. Hautojärvi P, Corbel C (1995) In: Dupasquier A, Mills AP (eds) Proceedings of the International School of Physics "Enrico Fermi", Course CXXV, IOS Press, Varena, 1995, p 491
27. Ribárik G, Gubicza J, Ungár T (2004) Mater Sci Eng A 387–389:343
28. Ungár T, Castelnau O, Ribárik G, Drakopoulos M, Béchade L, Chauveau T, Snigirev A, Snigireva I, Schroer C, Bacroix B (2007) Acta Mater 55:1117
29. Balogh L, Figueiredo RB, Ungár T, Langdon TG (2010) Mater Sci Eng A 528:533
30. Máthis K, Gubicza J, Nam NH (2005) J Alloys Compd 394:194
31. Janeček M, Yi S, Král R, Vrátná J, Kainer KU (2010) J Mater Sci 45:4665. doi:10.1007/s10853-010-4675-1
32. Barnett MR, Keshavarz Z, Beer AG, Atwell D (2004) Acta Mater 52:5093
33. Jain A, Agnew SR (2007) Mater Sci Eng A 462:29
34. AlMaharbi M, Karaman I, Beyerlein IJ, Foley DK, Hartwig T, Kecskes LJ, Mathaudhu SN (2011) Mater Sci Eng A 528:7616
35. Kim WJ, Hong SI, Kim YS (2003) Acta Mater 51:3293